

# Protective effects of CY-09 and astaxanthin on NaIO<sub>3</sub>-induced photoreceptor inflammation *via* the NLRP3/autophagy pathway

Xiao-Li Wang, Yun-Xia Gao, Qiong-Zhen Yuan, Ming Zhang

Department of Ophthalmology, West China Hospital, Sichuan University, Chengdu 610041, Sichuan Province, China

**Correspondence to:** Ming Zhang. Department of Ophthalmology, West China Hospital, Sichuan University, Chengdu 610041, Sichuan Province, China. mingzhangdoctor@163.com

Received: 2023-11-29 Accepted: 2024-04-11

## Abstract

• **AIM:** To study the effect of the NLRP3/autophagy pathway on the photoreceptor inflammatory response and the protective mechanism of CY-09 and astaxanthin (AST).

• **METHODS:** ICR mice were intraperitoneally injected NaIO<sub>3</sub>, CY-09, AST successively and divided into 5 groups, including the control, NaIO<sub>3</sub>, NaIO<sub>3</sub>+CY-09, NaIO<sub>3</sub>+AST, and NaIO<sub>3</sub>+CY-09+AST groups. Spectral domain optical coherence tomography and flash electroretinogram were examined and the retina tissues were harvested for immunohistochemistry, enzyme linked immunosorbent assay (ELISA), and Western blotting. Retinal pigment epithelium cell line (ARPE-19 cells) and mouse photoreceptor cells line (661W cells) were also treated with NaIO<sub>3</sub>, CY-09, and AST successively. Cell proliferation was assessed by cell counting kit-8 (CCK-8) assay. Apoptosis was analyzed by flow cytometry. Changes in autophagosome morphology were observed by transmission electron microscopy. Quantitative polymerase chain reaction (qPCR) was used to detect NLRP3 and caspase-1. NLRP3, caspase-1, cleaved caspase-1, p62, Beclin-1, and LC3 protein levels were measured by Western blotting. IL-1β and IL-18 were measured by ELISA.

• **RESULTS:** Compared with the control group, the activity of NaIO<sub>3</sub>-treated 661W cells decreased within 24 and 48h, apoptosis increased, NLRP3, caspase-1, IL-1β and IL-18 levels increased, and autophagy-related protein levels increased ( $P<0.05$ ). Compared with NaIO<sub>3</sub> group, CY-09 and AST inhibited apoptosis ( $P<0.05$ ), reduced NLRP3, caspase-1, IL-1β and IL-18 expression ( $P<0.05$ ), and inhibited autophagy. Compared with the other groups, CY-09 combined with AST significantly decreased NLRP3 expression and inhibited the

expression of the autophagy-related proteins p62, Beclin-1, and LC3 *in vitro* and *in vivo* ( $P<0.05$ ).

• **CONCLUSION:** CY-09 and AST inhibit NaIO<sub>3</sub>-induced inflammatory damage through the NLRP3/autophagy pathway *in vitro* and *in vivo*. CY-09 and AST may protect retina from inflammatory injury.

• **KEYWORDS:** CY-09; astaxanthin; retinal degeneration; photoreceptor cells; inflammation; NLRP3

**DOI:10.18240/ijo.2024.07.05**

**Citation:** Wang XL, Gao YX, Yuan QZ, Zhang M. Protective effects of CY-09 and astaxanthin on NaIO<sub>3</sub>-induced photoreceptor inflammation *via* the NLRP3/autophagy pathway. *Int J Ophthalmol* 2024;17(7):1217-1231

## INTRODUCTION

Retinal degenerative diseases are a group of chronic diseases that are characterized by the apoptosis of retinal photoreceptor cells, which leads to vision loss<sup>[1]</sup>. Chronic inflammation in the retina may be an important mechanism that initiates photoreceptor cell death in age-related macular degeneration (AMD)<sup>[2-3]</sup>. Intravitreal injection of vascular endothelial growth factor (VEGF) inhibitors is the first-line treatment for wet AMD<sup>[4-6]</sup>. But dry AMD that cannot be effectively controlled. When exposed to harmful stimuli, this retinal tissue activity may contribute to the establishment of a chronic inflammatory state in the local microenvironment<sup>[7]</sup> and abnormal immune activation may occur<sup>[8]</sup>. Photoreceptor cell death involves many molecular mechanisms, including NOD-, LRR- and pyrin domain-containing protein 3 (NLRP3) inflammasome-dependent pyroptosis<sup>[9-10]</sup>. Some studies have shown that the NLRP3/autophagy signaling pathway plays a key role in the inflammatory response of photoreceptors<sup>[11]</sup>. When stimulated, apoptosis-associated speck-like protein containing a caspase recruitment domain (ASC) play an important role in inflammasome activation<sup>[12]</sup>. When activated, NLRP3 cleaves pro-caspase-1 to its activated form, which further promotes the maturation of inflammatory precursor proteins to the activated forms of interleukin (IL)-1β and

IL-18<sup>[13-14]</sup>. Activated caspase-1 can also play a proinflammatory role<sup>[15-16]</sup>. There are three main mechanisms by which NLRP3 were activated: K<sup>+</sup> outflow<sup>[17-18]</sup>, the uptake of crystalline and particulate substances by phagocytes<sup>[19]</sup>, the production of reactive oxygen species (ROS)<sup>[20]</sup>. NaIO<sub>3</sub> can induce retinal pigment epithelium (RPE) cell death through mechanisms<sup>[21]</sup>. In adult retinal pigment epithelial cell line-19 (ARPE-19) cells, NLRP3 inhibitor can prevent NaIO<sub>3</sub>-induced lipid peroxidation, mitochondrial damage, DNA damage and cell death. In mouse models, NLRP3 inhibitor pretreatment can inhibit NaIO<sub>3</sub>-induced cell death<sup>[22]</sup>. In this study, the NLRP3 inhibitor CY-09 and astaxanthin (AST) were administered to study whether the combined treatment exerts anti-inflammatory and protective effects on photoreceptor cells and to elucidate the underlying mechanism.

## MATERIALS AND METHODS

**Ethical Approval** All the animal experiments were approved by the Ethics Committee of Animal Center, West China Hospital, Sichuan University (Ethics number: 20230406006) and were conducted in accordance with the Guiding Opinions on the Treatment of Laboratory Animals issued by the Ministry of Science and Technology of China.

**Cells and Animals** The cell lines included mouse photoreceptor cells (661W cells) and ARPE-19 cells were purchased from Guangzhou Ginio Biotechnology Co., Ltd., China. The ICR mice were 4-6 weeks old, weighed 25±3 g, and purchased from Beijing Huaifukang Company, China.

**Cell Culture** 661W cells were cultured in high-glucose Dulbecco's modified eagle medium (DMEM) supplemented with 10% fetal bovine serum (Hangzhou Tianhang Biotechnology Co., Ltd., China), 100 U/mL penicillin (HyClone, Logan, UT, USA), and 100 µg/mL streptomycin (HyClone). The ARPE-19 cells were cultured in DMEM/F-12 medium supplemented with 10% fetal bovine serum (Hangzhou Tianhang Biotechnology Co., Ltd., China), 100 U/mL penicillin (HyClone), and 100 µg/mL streptomycin (HyClone). The cells were cultured in an incubator in an environment with 5% CO<sub>2</sub>, saturated humidity and 37°C. When cell passage was performed, the cells were washed with phosphate buffer saline (PBS), and 2 mL of 0.25% pancreatic enzyme containing EDTA (Geno Biopharmaceutical Technology Co., Ltd., China) was added to digest the cells for 2-5min; then, the cells were centrifuged at 1000 rpm/min for 4min and resuspended for further experiments.

**Cell Counting Kit-8 Assay** The cells were cultured overnight in SHEL LAB and subjected to concentration gradients of NaIO<sub>3</sub> (0, 100, 300, 600, 900, 1200, 1500, 1800, and 2400 µg/mL). Then, three NaIO<sub>3</sub> concentrations were established and cell proliferation was analyzed after incubation with NaIO<sub>3</sub>. A

**Table 1 List of real-time polymerase chain reaction primer sequences**

Gene name	Nucleotide sequence (5'-3')
M-NLRP3-F	TCTCAAGTCTAAGCACCAACCG
M-NLRP3-R	CGAAGCAGCATTGATGGGAC
M-caspase-1-F	AGGGAATATGTGGGACCACATAC
M-caspase-1-R	CTGAATCTTTTAACAACACCCTCC
M-GAPDH-F	TGAAGGGTGGAGCCAAAAG
M-GAPDH-R	AGTCTTCTGGGTGGCAGTGAT
M-IL-1β-F	GAAATGCCACCTTTTGACAGTGAT
M-IL-1β-R	TTCTCCACAGCCACAATGAGT
M-IL-18-F	AGTTAGGTGGGAGGGTTTG
M-IL-18-R	ATCATGCAGCTCGGGTATT
M-Bax-F	CACTAAAGTGCCCGAGCTGA
M-Bax-R	GGTCCCGAAGTAGGAGAGGA

gradient design was carried out to expose cells to different concentrations of AST. Cells were cocultured with three concentrations of CY-09 and NaIO<sub>3</sub>. After the cells were culture under conventional conditions for 24, 48, and 72h, 10 µL cell counting kit-8 (CCK-8) solution was added and incubated at 37°C for 1-4h, and the absorbance was measured at 450 nm by a microplate system (Diatek Company., USA).

**Flow Cytometry** After cells were cultured overnight, NaIO<sub>3</sub>, CY-09, AST or a mixed solution containing the appropriate concentration was added to the cells. After incubation for 24h, the cells were transferred to 2 mL EP tubes and centrifuged. The cells were precipitated. Then 1 mL precooled PBS was added to resuspend the cells and centrifuged again. The cells were suspended in diluted binding buffer, and the concentration was adjusted to (1-5)×10<sup>6</sup> cells/mL. The cell suspensions were mixed with 5 µL of Annexin V/Alexa Fluor, and incubated at room temperature for 5min in the dark. Then, 10 µL and 20 µg/mL propidium iodide solution (Apoptosis kit: 4A BIOTECH Company., China) was added, 400 µL PBS was added, and the cells were immediately analyzed by flow cytometry.

**Quantitative Real-Time Polymerase Chain Reaction** A spectrophotometer was used to determine the concentration of the total RNA that was extracted. The total RNA samples were diluted in proportion, and subsequent quantitative real-time polymerase chain reaction (qPCR) experiments were immediately conducted. cDNA was then transcribed using a designed primer (Beijing Tsingke Biotech Co., Ltd., China) and gDNA Eraser (Vazyme Biotech Co., Ltd., China). qPCR was performed using the SYBR Green Master kit (Vazyme Biotech Co., Ltd., China) and fluorescent quantitative PCR apparatus (Life Technologies, USA). GAPDH was used as an endogenous control. The data were analyzed by the 2<sup>-ΔΔCT</sup> method (Table 1).

**Western Blotting** After cells were washed, RIPA lysis buffer (Beyotime Biotechnology Co., Ltd., China) containing

phosphatase inhibitor (ASPEN Biotechnology Co., Ltd., China) and protease inhibitor (Beyotime Biotechnology Co., Ltd., China) was added, and the cells were lysed on ice for 3-5min. The lysates were centrifuged at 12 000 g and 4°C for 5min. The protein concentrations were determined with a BCA kit (Beyotime Biotechnology Co., Ltd., China). Before the protein loading buffer (Bio-Rad Laboratories Co., Ltd., USA) was used,  $\beta$ -mercaptoethanol was added and mixed. Then, 4 $\times$  loading buffer was added, mixed, and incubated in a 100°C water bath for 10min. The SDS-PAGE gel (BIOSHARP Company, China) was prepared. The appropriate SDS-PAGE separation gel was selected according to the molecular weights of the target proteins. The sample proteins and the protein prestained marker (Beyotime Biotechnology Co., Ltd., China) were added to the sample wells of an SDS-PAGE gel, and electrophoresis was carried out at 80 V for 30min. After electrophoresis, the proteins were transferred to polyvinylidene fluoride (PVDF) membranes (Merck, USA) and marker position to make the sandwich for protein transfer. After transfer, the PVDF membranes were incubated in 50 mL of 5% skim milk (BD Company, USA) on a shaker for 1-2h. Then, primary antibodies were diluted in PBS with Tween-20 (PBST), added to the membranes, and incubated at 4°C overnight. The primary antibodies included the following: rabbit anti-NLRP3 antibody (US CST Corporation, USA, #15101), rabbit anti-caspase-1 antibody (Affbiotech, AUS #AF5418), rabbit anti-cleaved caspase-1 antibody (Affbiotech, #AF4005), rabbit anti-P62 antibody (CST Corporation, #39749), rabbit anti-Beclin-1 antibody (CST Corporation, #3495), rabbit anti-LC-3 antibody (CST Corporation, #4108), and rabbit anti-GAPDH antibody (Abcam Corporation, UK, # ab181602). Then, the primary antibodies were removed, and were washed with PBST 3 times for 5min each. The corresponding diluted fluorescent secondary antibodies (LI-COR Corporation, USA) were added and incubated at room temperature for 1h in the dark. Then, the PVDF membranes were washed with PBST in the dark and immediately placed in a Western blotting image analysis system to collect and save images.

**Immunofluorescence Staining** Cellular immunofluorescence was performed according to standard procedures, which included cell preparation, fixation, permeabilization, blocking, primary antibody incubation, secondary antibody incubation, washing, mounting, observation and imaging.

**Enzyme-Linked Immunosorbent Assay** Enzyme-linked immunosorbent assay (ELISA) was performed following the steps in the kit instructions (ELK Biotechnology, China). These steps included coating, blocking, sample addition, primary antibody binding, washing, secondary antibody binding,

substrate addition, reaction termination, detection and analysis.

**Establishment of the Animal Model** The experimental animals were raised in the standard specific pathogen free (SPF) environment. NaIO<sub>3</sub> powder was dissolved at a concentration of 12.5 mg/mL (4 mL). The mice were divided into different group (25, 50, and 100 mg/kg), and NaIO<sub>3</sub> was delivered by intraperitoneal injection. Experimental mice were randomly divided into 5 groups, included the control group, NaIO<sub>3</sub> group, NaIO<sub>3</sub>+CY-09 group, NaIO<sub>3</sub>+AST group and NaIO<sub>3</sub>+CY-09+AST group. CY-09 powder was dissolved in a solution containing 10% DMSO+90% corn oil. The AST was dissolved in PBS by ultrasonication for 15min. In the treatment groups, NaIO<sub>3</sub> solution was intraperitoneally administered only once. CY-09 was intraperitoneally starting on the second day after the establishment of the model and continued for 1wk. AST was continuously administered for 1wk starting on the second day after the establishment of the model.

**Hematoxylin and Eosin Staining** Tissues were fixed with formalin. Then, the tissues were washed with PBS to remove the fixative. Then, the tissues were dehydrated with a series of graded alcohol solutions and were stained with hematoxylin to stain the cell nuclei, followed by eosin to stain the cytoplasm. Then were treated with a clearing agent such as xylene to render them transparent. The slides then were mounted with neutral balsam, and were observed under a microscope.

**Spectral Domain Optical Coherence Tomography** Fundus imaging was performed with spectral domain optical coherence tomography (SD-OCT) to evaluate changes in retinal layers from model mice. All the examinations were performed by the intraperitoneal injection of tribromoethanol solution under general anesthesia. The examinations were carried out on the 3<sup>rd</sup> and 7<sup>th</sup> day after treatment.

**Flash Electroretinogram** On the 3<sup>rd</sup> and 8<sup>th</sup> day, flash electroretinogram (FERG) was performed under the conditions of light adaptation (LA) and dark adaptation (DA). All the examinations were performed under general anesthesia. First, DA examination was performed, in which the mice were exposed to stimulation ranging from low to high, and then, LA examination was performed. After the test, the latent value and amplitude value of the FERG a and b waves were measured and evaluated by the same experienced ophthalmologist.

**Statistical Analysis** SPSS and GraphPad Prism 9 were used for statistical description and analysis. Measurement data with normal distribution were presented as the mean $\pm$ standard deviation (SD). One-way analysis of variance (ANOVA) was used for comparisons of more than two groups and then multiple comparison of LSD, and the difference between two groups was analyzed by Student's *t*-test. *P*<0.05 was considered statistical significance.

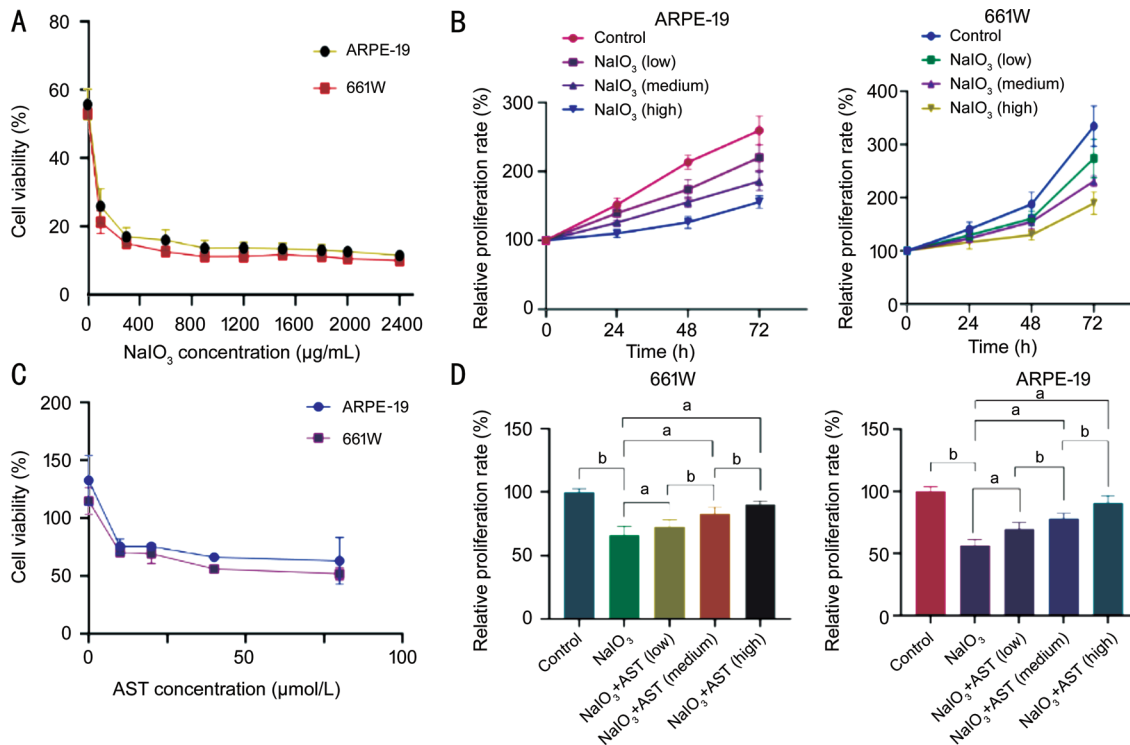


**Figure 1** Effects of NaIO<sub>3</sub> and AST on 661W and ARPE-19 cells. A: Proliferation of 661W and ARPE-19 cells after treatment with different concentrations of NaIO<sub>3</sub>; B: Proliferation of 661W and ARPE-19 cells after treatment with NaIO<sub>3</sub> for different times; C: Activity of 661W and ARPE-19 cells after treatment with different concentrations of AST; D: Proliferation of 661W and ARPE-19 cells after treatment with AST+NaIO<sub>3</sub> at three concentrations. AST: Astaxanthin; 661W: Mouse photoreceptor cells line; ARPE-19: Adult retinal pigment epithelial cell line-19. <sup>a</sup>*P*<0.05, <sup>b</sup>*P*<0.01.

## RESULTS

### Effects of NaIO<sub>3</sub>, CY-09, and AST on 661W and ARPE-19 Cells Proliferation and Activity

In the cell proliferation experiment, and concentrations of 0, 100, 300, 600, 900, 1200, 1500, 1800, 2100, and 2400 µg/mL NaIO<sub>3</sub> was tested. Then, three different concentrations of NaIO<sub>3</sub> within the appropriate range, 250, 500, and 750 µg/mL NaIO<sub>3</sub>, were tested at time points of 24, 48, and 72h (Figure 1A). The results suggested that the medium concentration and high concentration of NaIO<sub>3</sub> caused cell damage after 24h and 72h of treatment, and cell proliferation was inhibited at the lower concentration (Figure 1B). The AST concentrations included 0, 10, 20, 40, and 80 µmol/L, and the cells were cocultured with 500 µg/mL NaIO<sub>3</sub> solution for 24h (Figure 1C). Then, low, medium and high concentrations of AST (5, 10, and 20 µmol/L) were chosen and combined with 500 µg/mL NaIO<sub>3</sub> to treat 661W cells and ARPE-19 cells. It was found that with increasing AST concentration, cell activity increased (Figure 1D).

Three different concentrations of CY-09 (25, 50, and 100 µmol/L) and 500 µg/mL NaIO<sub>3</sub> solution were combined and incubated with 661W cells. Compared with the NaIO<sub>3</sub> group, the cell activity increased with CY-09 concentration increasing (Figure 2A). In the control group, the apoptosis rate of 661W cells was 6.82%, and ARPE-19 cells was 7.15%. When NaIO<sub>3</sub> was administered, the average apoptosis rate of 661W cells was

32.28%, and ARPE-19 cells was 23.25%. When NaIO<sub>3</sub>+CY-09 was administered, the mean apoptosis rate of 661W cells was 23.11%, and ARPE-19 cells was 20.90%. These results showed that with the addition of CY-09, the apoptosis rate of the two kinds of cells was decreased compared with that in NaIO<sub>3</sub> group (*P*<0.01; Figure 2B).

The immunofluorescence staining results in 661W cells showed that a small amount of NLRP3 was uniformly expressed in the cytoplasm of the control group, and the cells were densely distributed. After NaIO<sub>3</sub> treatment, cell death was increased and the green fluorescence in the cells was enhanced. The fluorescence of the NaIO<sub>3</sub>+CY-09 group was decreased (Figure 2C).

**Effect of CY-09 Combined with Astaxanthin on Inflammatory Response and Apoptosis of 661W and ARPE-19 Cells** ELISA results showed that the levels of IL-1β and IL-18 in the NaIO<sub>3</sub> group were significantly increased than in the control group (*P*<0.05) and decreased in NaIO<sub>3</sub>+CY-09 and NaIO<sub>3</sub>+AST group (*P*<0.05) especially in the NaIO<sub>3</sub>+CY-09+AST group (*P*<0.05) both in 661W and ARPE-19 cells (Figure 2D, 2E).

In the control group, the apoptosis rate of 661W cells was 5.05%, and ARPE-19 cells was 6.33%. In the NaIO<sub>3</sub> group, the apoptosis rate of 661W cells was 31.55%, and ARPE-19 cells was 30.33%. In the NaIO<sub>3</sub>+CY-09 group, the apoptosis rate of

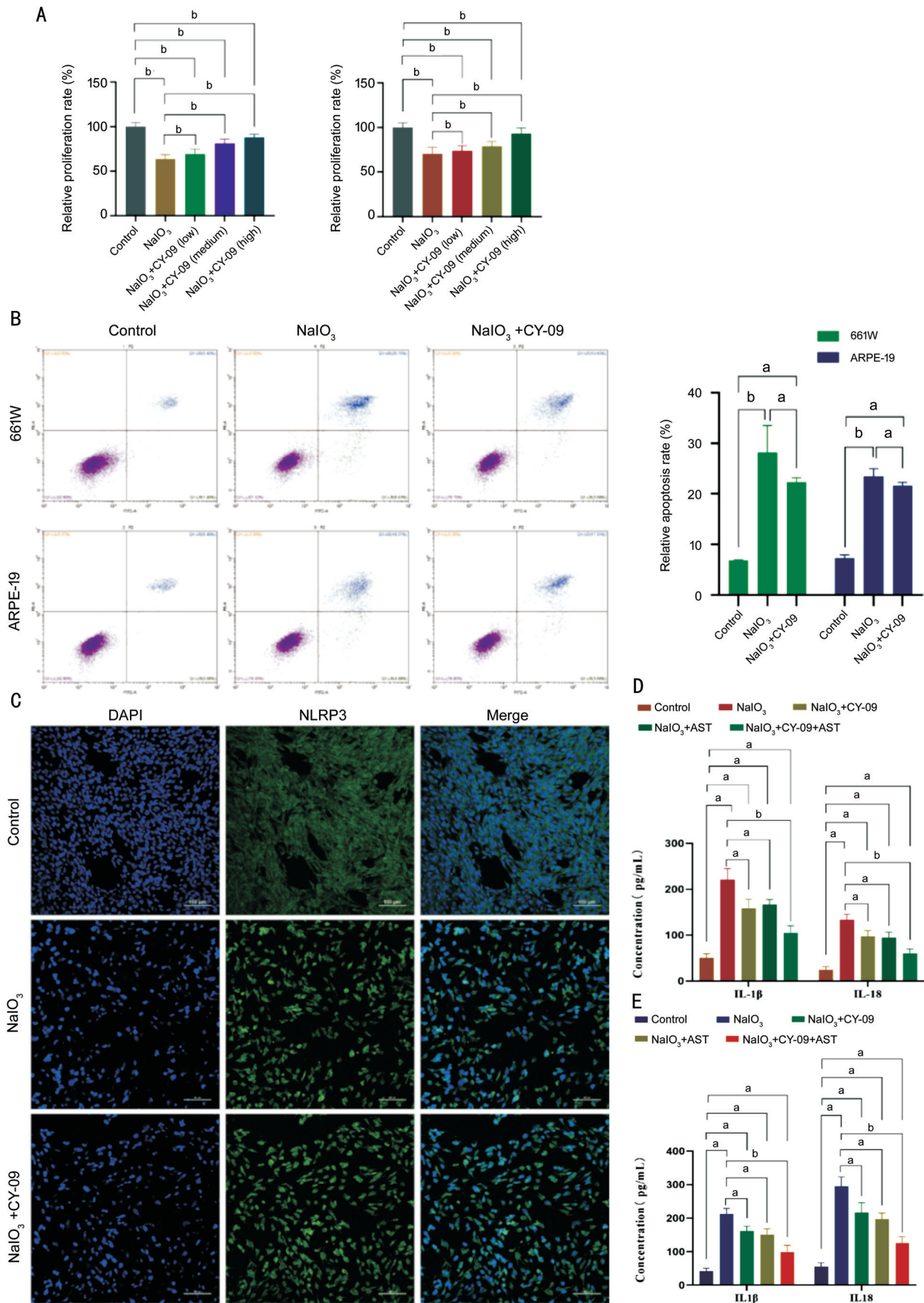


**Figure 2** Effects of NaIO<sub>3</sub> and CY-09 on 661W and ARPE-19 cells. A: Compared with the NaIO<sub>3</sub> group, the cell activity increased with increasing CY-09 concentration in 661W and ARPE-19 cells; B: Apoptosis of 661W and ARPE-19 cells after treatment with NaIO<sub>3</sub> and CY-09; C: NLRP3 expression by immunofluorescence after CY-09 treatment in the 661W cell; D, E: Expression of IL-1β and IL-18 in 661W (D) and ARPE-19 (E) cells treated with CY-09 combined with AST using ELISA. <sup>a</sup>P<0.05, <sup>b</sup>P<0.01. 661W: Mouse photoreceptor cells line; ARPE-19: Adult retinal pigment epithelial cell line-19; NLRP3: NOD-, LRR- and pyrin domain-containing protein 3; CY-09: An inhibitor binds to NLRP3; IL: Interleukin; AST: Astaxanthin.

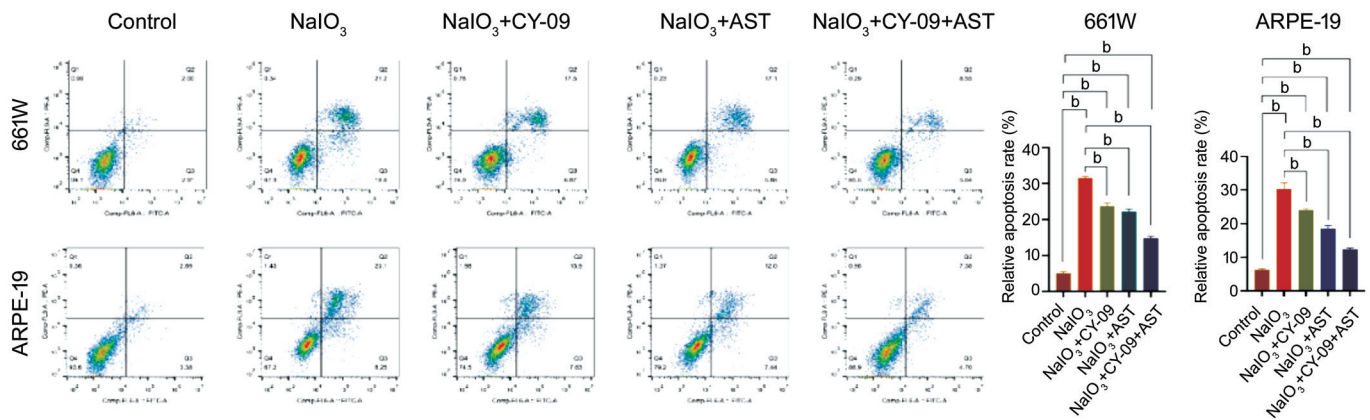


**Figure 3** 661W and ARPE-19 cell apoptosis after treatment with CY-09 combined with AST <sup>b</sup>*P*<0.01. 661W: Mouse photoreceptor cells line; ARPE-19: Adult retinal pigment epithelial cell line-19; NLRP3: NOD-, LRR- and pyrin domain-containing protein 3; AST: Astaxanthin; CY-09: An inhibitor binds to NLRP3.

661W cells was 23.64%, and ARPE-19 cells was 24.00%. In the NaIO<sub>3</sub>+AST group, the apoptosis rate of 661W cells was 22.17%, and ARPE-19 cells was 18.54%. In the NaIO<sub>3</sub>+CY-09+AST group, the apoptosis rate of 661W cells was 14.79%, and ARPE-19 cells was 12.43%. These results showed that with the addition of CY-09 and AST, the apoptosis rates of these two kinds of cells were decreased compared with those that were treated with NaIO<sub>3</sub> alone (*P*<0.01; Figure 3).

The mRNA levels of NLRP3 and caspase-1 in NaIO<sub>3</sub> group were higher than in the control group (*P*<0.05) in 661W cell, and decreased in NaIO<sub>3</sub>+CY-09 and NaIO<sub>3</sub>+AST group, especially in NaIO<sub>3</sub>+CY-09+AST group (*P*<0.05; Figure 4A). The protein levels of NLRP3 and cleaved caspase-1 also decreased in NaIO<sub>3</sub>+CY-09, NaIO<sub>3</sub>+AST, and NaIO<sub>3</sub>+CY-09+AST group (Figure 4B).

**Effect of CY-09 Combined with Astaxanthin on Autophagy in 661W and ARPE-19 Cells** Compared with the NaIO<sub>3</sub> group, the expression of p62 in NaIO<sub>3</sub>+CY-09 and NaIO<sub>3</sub>+AST groups were increased in both 661W and ARPE-19 cells (*P*<0.05), while Beclin-1, LC3-I, LC3-II, and LC3-II/LC3-I were decreased (*P*<0.05), especially in NaIO<sub>3</sub>+CY-09+AST group (*P*<0.05; Figure 5).

Electron microscopy images of 3400×, 8500×, and 17500× of 661W cells showed that the control group had a few autophagosomes that were generally not large. In the NaIO<sub>3</sub> group, there were obvious, large bulla-like autophagosomes and more fusion occurred. In the NaIO<sub>3</sub>+CY-09 and NaIO<sub>3</sub>+AST groups, the number of fused autophagosomes was significantly reduced compared with that in the NaIO<sub>3</sub> group. The number of autophagosome vesicles in the NaIO<sub>3</sub>+CY-09+AST group was reduced compared with that in the other treatment groups (Figure 6).

**Establishment of an AMD Model by NaIO<sub>3</sub> Injection** On the 3<sup>rd</sup> day, retinal pigment disorder was observed in the high-dose group. In the medium-dose group, retinal

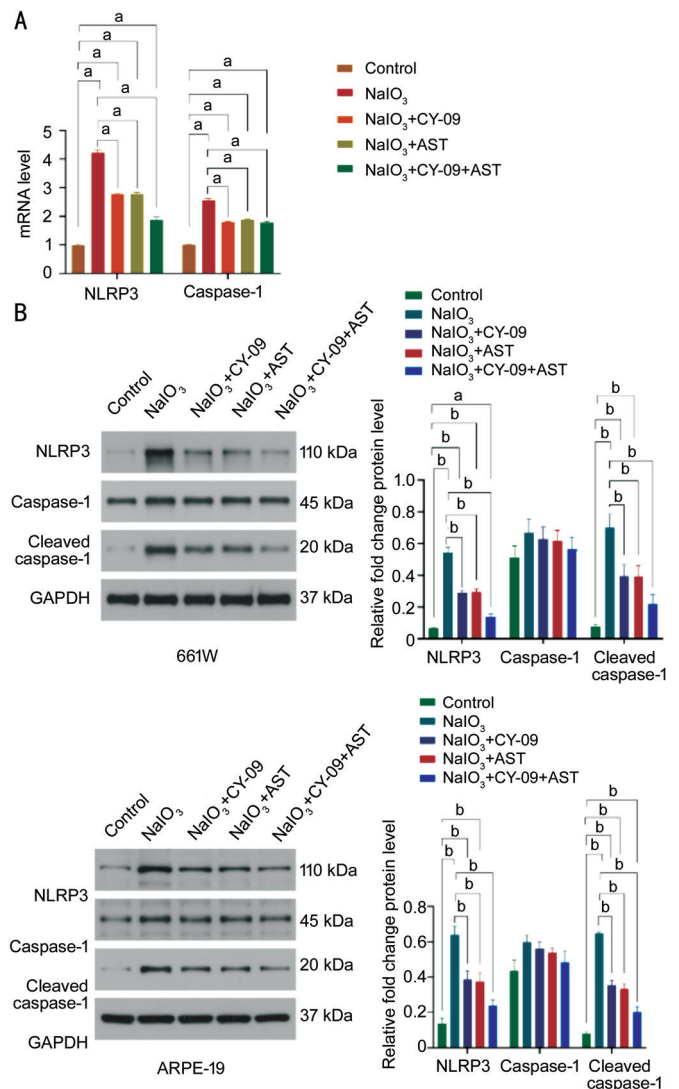


**Figure 4** Effects of AST and CY-09 on NLRP3, caspase-1 expression in 661W and ARPE-19 cells A: The mRNA levels of NLRP3 and caspase-1 in 661W cells; B: The protein levels of NLRP3 and cleaved caspase-1 in 661W and ARPE-19 cells. <sup>a</sup>*P*<0.05, <sup>b</sup>*P*<0.01. 661W: Mouse photoreceptor cells line; ARPE-19: Adult retinal pigment epithelial cell line-19; NLRP3: NOD-, LRR- and pyrin domain-containing protein 3; AST: Astaxanthin; CY-09: An inhibitor binds to NLRP3.

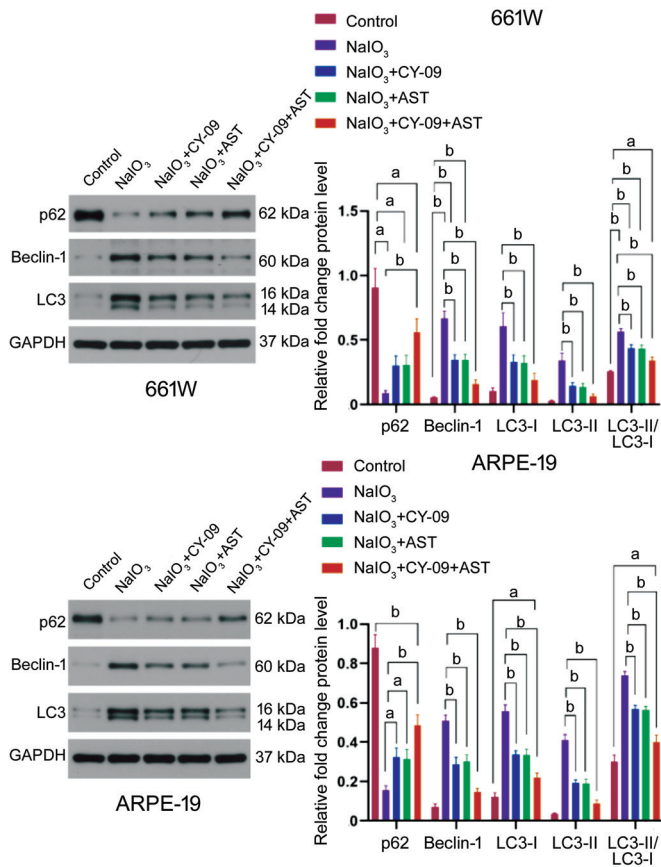


**Figure 5** Effects of AST and CY-09 on autophagy-related protein expression in 661W and ARPE-19 cells <sup>a</sup>*P*<0.05, <sup>b</sup>*P*<0.01. 661W: Mouse photoreceptor cells line; ARPE-19: Adult retinal pigment epithelial cell line-19; NLRP3: NOD-, LRR- and pyrin domain-containing protein 3; AST: Astaxanthin; CY-09: An inhibitor binds to NLRP3.

pigment disorder and interlayer highly reflective spots in the corresponding area were observed. In the low-dose group, there were a few interlayer spots. On the 7<sup>th</sup> day, the retina of all groups exhibited retinal background pigment disruption and more interlayer dots (Figure 7).

Dark adaptation was mainly tested with different intensities of flash stimulation. The test conditions were as follows: DQQ DA 0.001, DQQ DA 0.01, DQQ DA 0.1, DQQ DA 1.0, DQQ DA 3.0, DQQ DA 3.0 OP, DQQ DA 10.0, and DQQ LA 3.0. The wave amplitudes and latency of the a- and b-waves in the control group were normal, and the wave amplitudes of the low-dose group, medium-dose group and high-dose group were decreased to different degrees (Figure 8).

Due to the influence of drug injection and anesthesia, the mortality rates were higher. Only the eyes of mice from the control group and low-dose group were harvested for hematoxylin and eosin (HE) and immunohistochemical staining. In the control group, the structure of retinal layers was clear, the retinal nerve layer were neatly arranged, cell morphology was good and the staining was uniform. In the NaIO<sub>3</sub> group, the retinal layer structure was obviously loose, the structure was not orderly, cell staining was not uniform,

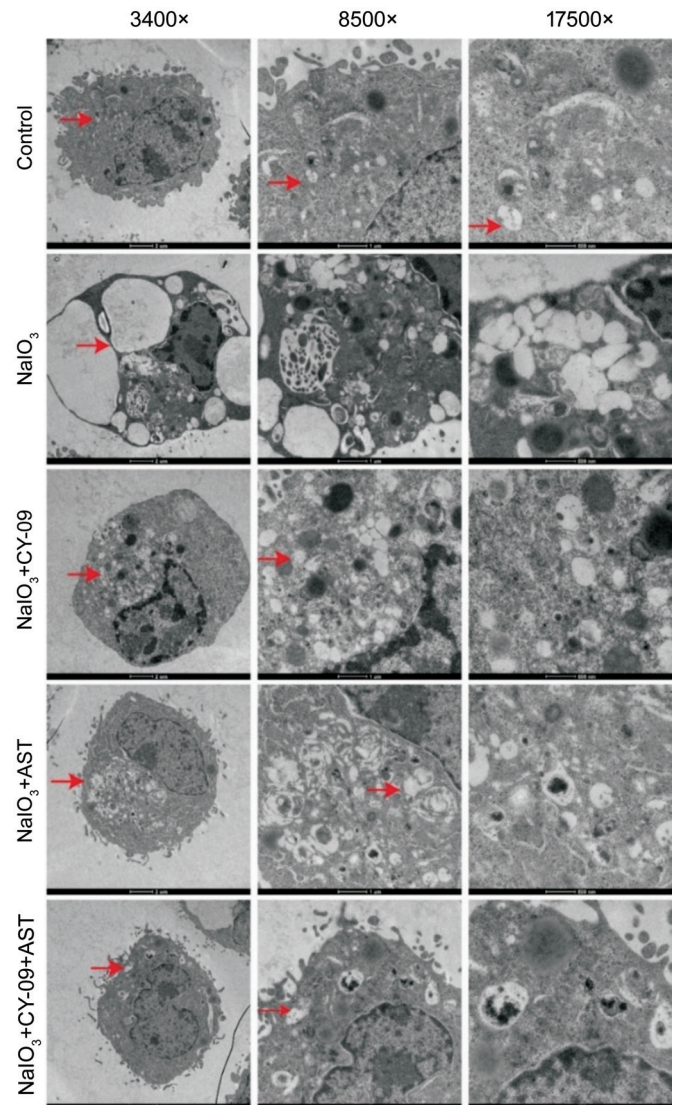


**Figure 6** Morphological changes in autophagosomes in different groups of 661W cells after treatment 661W: Mouse photoreceptor cells line; AST: Astaxanthin; CY-09: An inhibitor binds to NLRP3; NLRP3: NOD-, LRR- and pyrin domain-containing protein 3.

and some cells were irregular, swollen, displaced or absent (Figure 9).

**Expression of NLRP3 and Inflammatory Factors as well as Autophagy in Mouse** The retinal background image of the control group is clear, and the structure of each layer is clear and complete. In the NaIO<sub>3</sub> group, the retinal structure was thin, there were more high reflection points between layers, and the RPE layer changed unevenly. The NaIO<sub>3</sub>+CY-09 group had uneven pigment disorder and a high interlayer dot reflex. The NaIO<sub>3</sub>+AST group exhibited uneven, disordered changes in pigment, and the retinal interlayer had slightly more spot-like high reflexes. The NaIO<sub>3</sub>+CY-09+AST group had uneven, disordered changes in pigment (Figure 10).

The experimental mice were examined with FERG to evaluate the functional changes in the retina after different treatments (Figure 11).

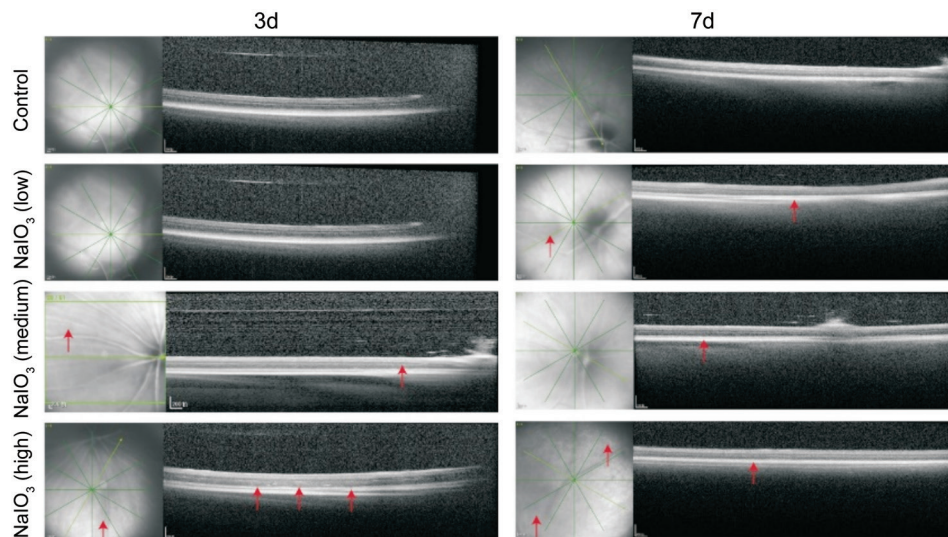


**Figure 7** SD-OCT images after NaIO<sub>3</sub> administration SD-OCT: Spectral domain optical coherence tomography.

In control group, the retinal tissue of mouse eyeballs showed complete structure, clear layers, close arrangement of cells, uniform and good staining, clear and good cell morphology. In treated groups, the structure of retinal layers was disordered and relaxed, the RPE pigment was disordered and displaced, and local photoreceptor cells were moved, resulting in unclear structure of retinal layers, irregular cell morphology, deformation and expansion. In the NaIO<sub>3</sub>+CY-09 group the retinal structure of each layer could be distinguished. In the NaIO<sub>3</sub>+AST group, retinal relaxation, RPE structure and pigment detachment were observed, and nuclear staining was obvious. The structure of each layer in the NaIO<sub>3</sub>+CY-09+AST group was improved (Figure 12).

NLRP3 was increased in the NaIO<sub>3</sub> group, and the number of positive areas increased. The positive expression and region of positive expression in the NaIO<sub>3</sub>+CY-09 and NaIO<sub>3</sub>+AST groups were decreased compared with those in the NaIO<sub>3</sub> group. The positive expression and region of positive expression in the NaIO<sub>3</sub>+CY-09+AST group were decreased compared with those in the NaIO<sub>3</sub>, NaIO<sub>3</sub>+CY-09 and NaIO<sub>3</sub>+AST groups. Caspase-1 staining revealed positive expression in the NaIO<sub>3</sub> group, NaIO<sub>3</sub>+CY-09 group, NaIO<sub>3</sub>+AST group and NaIO<sub>3</sub>+CY-09+AST group with a large regions of positive staining (Figure 13).

IL-1 $\beta$  and IL-18 in the NaIO<sub>3</sub>+CY-09 group were lower than in the NaIO<sub>3</sub> group ( $P<0.05$ ). IL-1 $\beta$  and IL-18 in the NaIO<sub>3</sub>+AST group were lower than in the NaIO<sub>3</sub>+CY-09 group ( $P<0.05$ ). IL-1 $\beta$  and IL-18 in the NaIO<sub>3</sub>+CY-09+AST group were decreased compared with all the other groups ( $P<0.05$ ; Figure 14). Compared with that in the NaIO<sub>3</sub> group, NLRP3 was decreased in the other treatment groups; that in the NaIO<sub>3</sub>+CY-09 group was lower than in the NaIO<sub>3</sub> group ( $P<0.01$ ). The NaIO<sub>3</sub>+CY-09+AST group had lower NLRP3 expression than all the other groups ( $P<0.05$ ). Caspase-1 in all the other groups was

reduced compared with that in the NaIO<sub>3</sub> group ( $P<0.05$ ). The NaIO<sub>3</sub>+CY-09 group had lower caspase-1 than the NaIO<sub>3</sub> group ( $P<0.01$ ). The NaIO<sub>3</sub>+CY-09+AST group had lower caspase-1 than the NaIO<sub>3</sub>+CY-09 group and NaIO<sub>3</sub>+AST group ( $P<0.05$ ). Compared with that in the NaIO<sub>3</sub> group, p62 in the other treatment groups was increased ( $P<0.05$ ). The NaIO<sub>3</sub>+CY-09+AST group exhibited higher p62 than the NaIO<sub>3</sub>+CY-09 group and NaIO<sub>3</sub>+AST group ( $P<0.05$ ). Compared with NaIO<sub>3</sub> group, Beclin-1 in the other treatment groups was decreased ( $P<0.05$ ). The NaIO<sub>3</sub>+CY-09+AST exhibited lower LC3-II/LC3-I than the NaIO<sub>3</sub>+CY-09 group and NaIO<sub>3</sub>+AST group ( $P<0.05$ ; Figure 15).

## DISCUSSION

Retinal photoreceptor cells can directly convert external light into visual signals<sup>[23]</sup>. The damage and death of photoreceptor cells are important causes of visual loss in AMD<sup>[24]</sup>. Aging can induce retinal inflammation, which evolves into a chronic inflammatory state<sup>[25]</sup>. Photoreceptor cell death involves a variety of molecular mechanisms related to cell death, including inflammation and apoptosis; among these processes which includes the NLRP3 inflammasome as the core cell death pathway, photoreceptor autophagy and ferroptosis pathway<sup>[26]</sup>. Dry AMD is closely related to the NLRP3 inflammasome and autophagy<sup>[27]</sup>.

There is currently no effective treatment for dry AMD<sup>[6]</sup>. The currently available animal models can simulate many pathological features of human AMD<sup>[28]</sup> and have their own diversity, advantages and limitations<sup>[29]</sup>. In this study, we chose NaIO<sub>3</sub> induction to establish AMD models. This model can selectively cause RPE cell damage, making it a replicable<sup>[30]</sup>. NaIO<sub>3</sub> induces retinal tissue senescence *in vivo*, significant age-related DNA damage in cells<sup>[31]</sup>. Therefore, in this study, 661W cells and ARPE-19 cells were treated with NaIO<sub>3</sub>, and NaIO<sub>3</sub> was administered to mice *via* intraperitoneal injection.

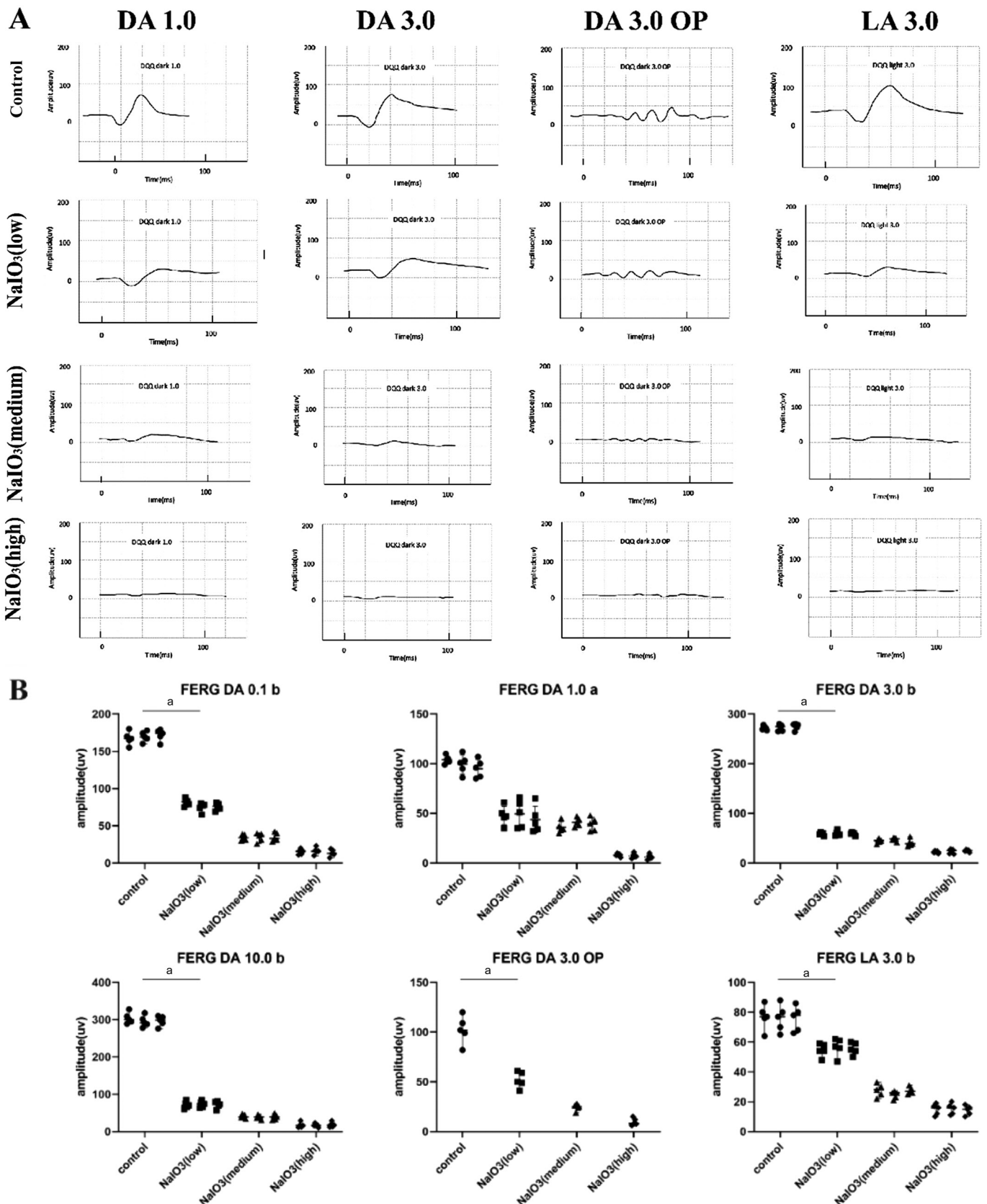


**Figure 8** Analysis of FERG images captured on the 8<sup>th</sup> day after NaIO<sub>3</sub> infusion A: Waveform of each group after model establishment; B: Statistical analysis of the amplitudes of the wave. <sup>a</sup>P<0.05. FERG: Flash electroretinogram; DA: Dark adaptation; LA: Light adaptation.

Animal experiments were also performed with different doses. The study showed that the retinal thickness of the model group was reduced, the a-wave and b-wave of FERG were decreased, the cell level was disordered, the photosensitive cells in the

outer plexiform layer were denatured, all the layers of the retina were affected, and visual function was affected. The results showed that NaIO<sub>3</sub>-induced *in vivo* and *in vitro* AMD models were successfully and feasibly established, and these

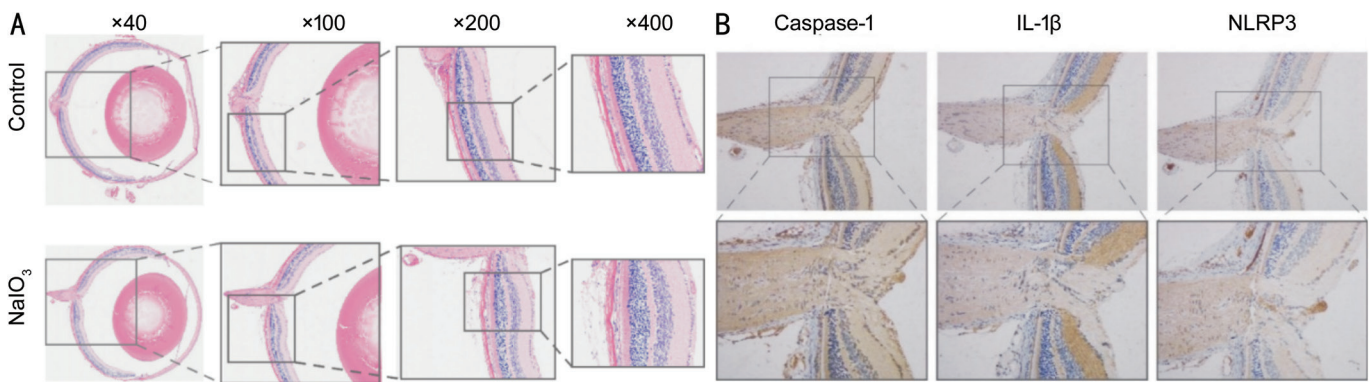


**Figure 9 Preliminary pathological sectioning after NaIO<sub>3</sub> infusion** A: Hematoxylin and eosin staining; B: Immunohistochemical staining. IL: Interleukin; NLRP3: NOD-, LRR- and pyrin domain-containing protein 3.

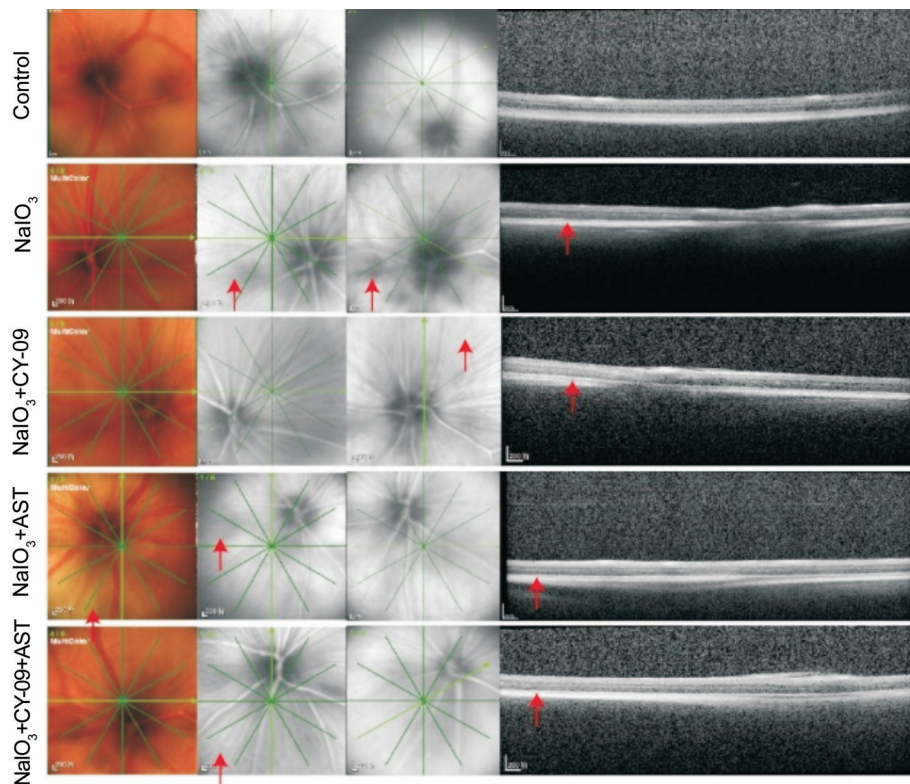


**Figure 10 Retinal SD-OCT images of mice from each group after combined treatment** SD-OCT: Spectral domain optical coherence tomography; AST: Astaxanthin; CY-09: An inhibitor binds to NLRP3; NLRP3: NOD-, LRR- and pyrin domain-containing protein 3.

models could be used for further experimental exploration. Senescence, metabolism, inflammation and oxidative damage of photoreceptor cells and RPE may be related to AMD. Treatment of mice and cultured retinal cells, including 661W cells and ARPE-19 cells, with NaIO<sub>3</sub> significantly reduced photoreceptor cell function<sup>[32]</sup>. NaIO<sub>3</sub> reduced b-wave amplitude and retinal thickness, leading to a loss of normal RPE hexagonal shape<sup>[33]</sup>. After NLRP3 is activated, it can promote the recruitment of activate caspase-1 which can promote the secretion of IL-1β<sup>[34]</sup>. *In vitro*, NaIO<sub>3</sub> activated several cell death pathways in retinal cells<sup>[35]</sup>. This result was also observed in this study. The expression levels of IL-1β and IL-18 were significantly upregulated. Increased expression of NLRP3, caspase-1, and cleaved caspase-1 were observed.

The levels of IL-1β and IL-18 were decreased, indicating that the combination of drugs had a certain inhibitory effect on inflammatory factor production. The transcription levels of NLRP3 and caspase-1 confirmed that CY-09 and AST exerted a certain inhibitory effect on the NaIO<sub>3</sub>-induced inflammatory response, and the inhibitory effect of drug combination was stronger. Apoptosis experiments also confirmed that. In terms of protein expression, the same conclusion was obtained for the NLRP3, caspase-1, and cleaved caspase-1. The expression of autophagy-related proteins and observe the autophagic flux with electron microscopy, were employed<sup>[36]</sup>. When the LC3 protein in the outer membrane of autophagic vesicles is fused with a fluorescent protein, it can be localized in the cell<sup>[37]</sup>. The change in autophagy can be measured

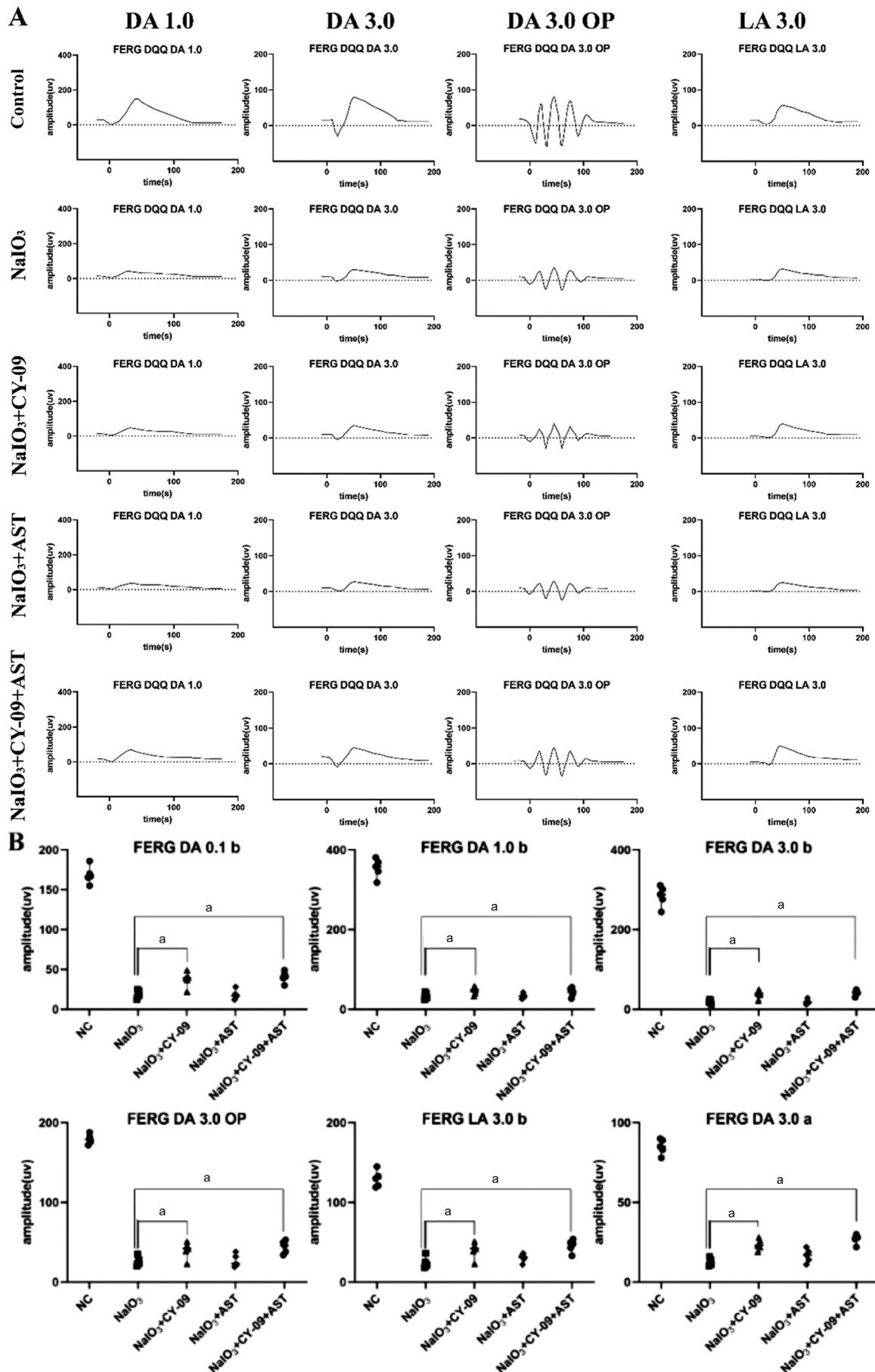


**Figure 11** Visual electrophysiological evaluation of retinal function in mice after treatment A: Retinal electrophysiological waveforms of mice from each group 10d after treatment; B: Statistical analysis of the amplitudes of waves in each group. <sup>a</sup>*P*<0.05. FERG: Flash electroretinogram; AST: Astaxanthin; CY-09: An inhibitor binds to NLRP3; NLRP3: NOD-, LRR- and pyrin domain-containing protein 3; DA: Dark adaptation; LA: Light adaptation.

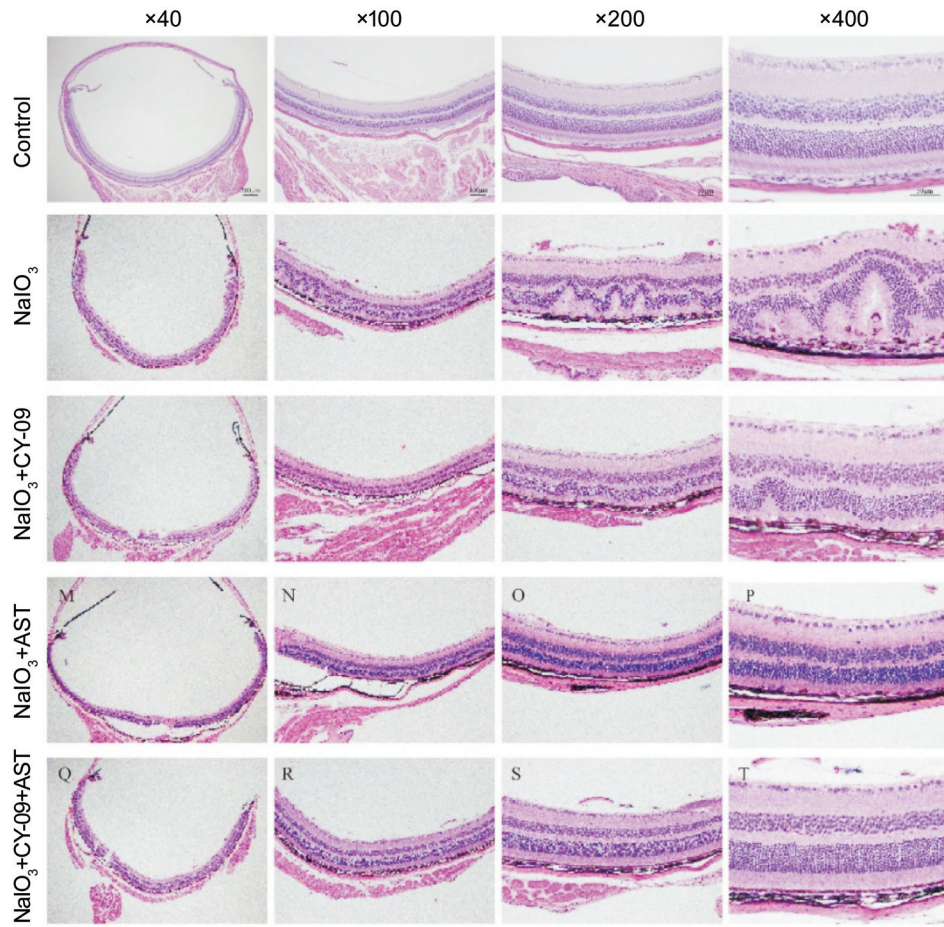


**Figure 12 HE staining of retinal tissues after different treatments** HE: Hematoxylin and eosin; AST: Astaxanthin; CY-09: An inhibitor binds to NLRP3; NLRP3: NOD-, LRR- and pyrin domain-containing protein 3.

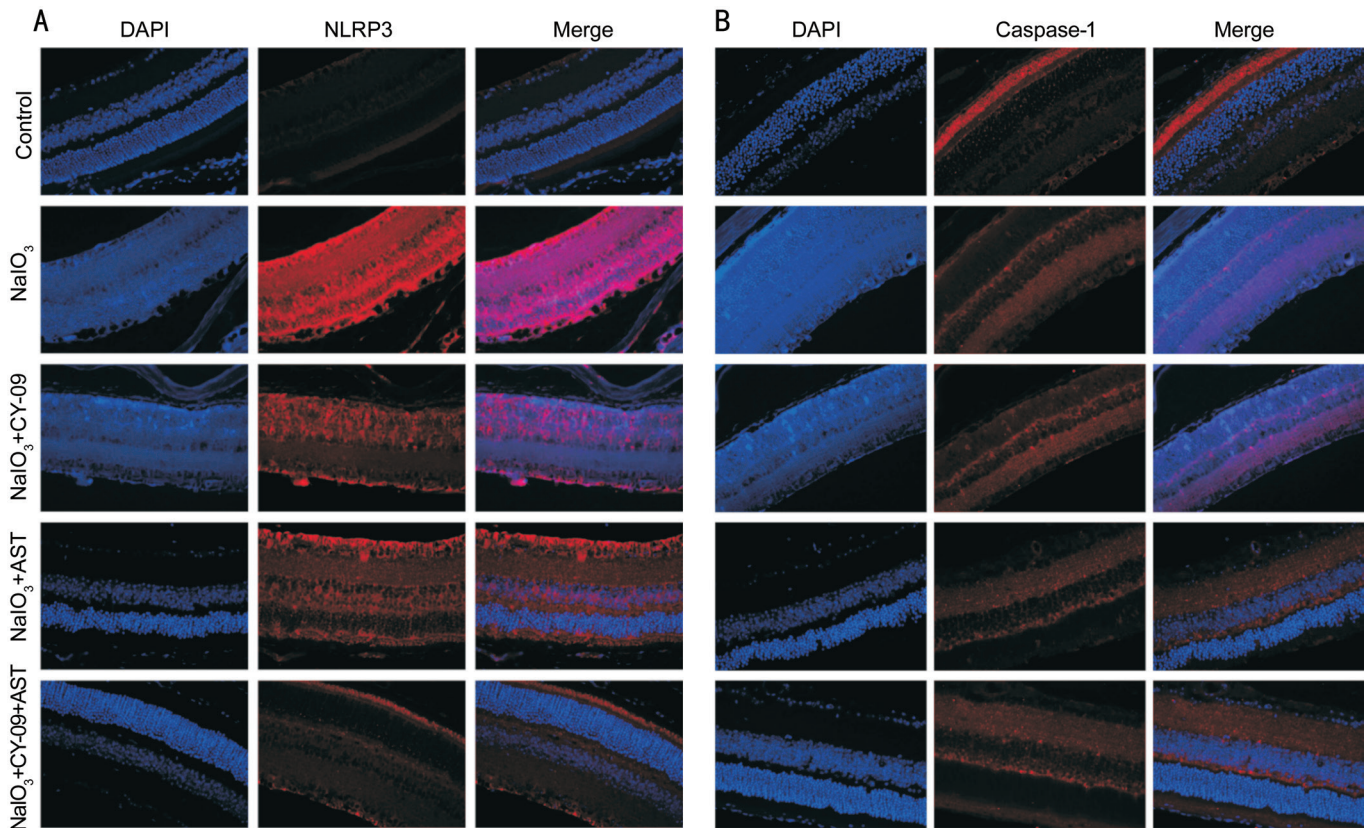


**Figure 13 Immunofluorescence staining of NLRP3 (A) and caspase-1 (B) in retinal tissues after different treatments** AST: Astaxanthin; CY-09: An inhibitor binds to NLRP3; NLRP3: NOD-, LRR- and pyrin domain-containing protein 3.

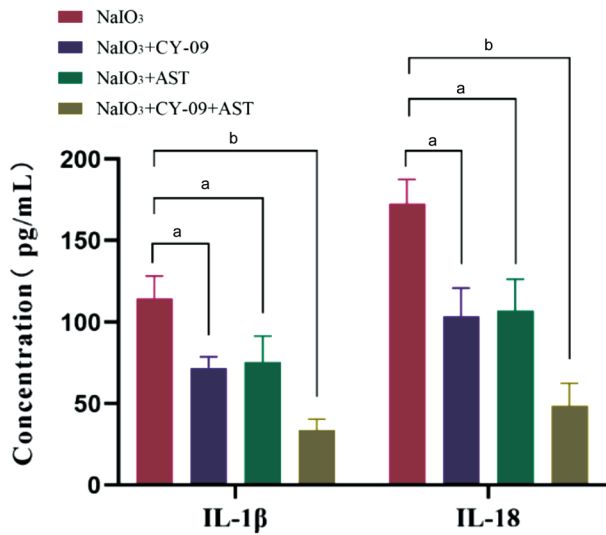


**Figure 14 IL-1 $\beta$  and IL-18 expression in retinal tissues after different treatments using ELISA** <sup>a</sup> $P$ <0.05, <sup>b</sup> $P$ <0.01. IL: Interleukin; AST: Astaxanthin; CY-09: An inhibitor binds to NLRP3; NLRP3: NOD-, LRR- and pyrin domain-containing protein 3.

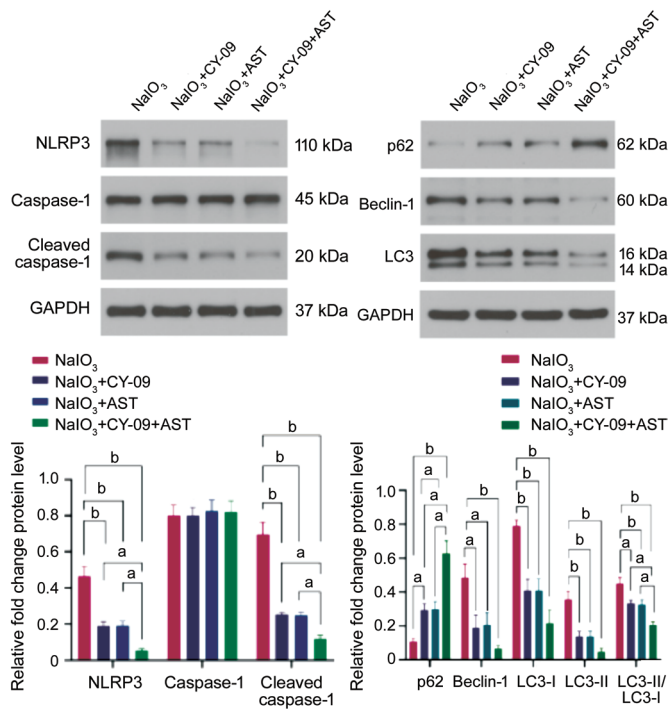


**Figure 15 Effects of AST and CY-09 on NLRP3, caspase-1, and autophagy-related protein expression in mice** <sup>a</sup> $P$ <0.05, <sup>b</sup> $P$ <0.01. NLRP3: NOD-, LRR- and pyrin domain-containing protein 3; AST: Astaxanthin; CY-09: An inhibitor binds to NLRP3.

by observing the number of substrate residues that are not degraded in phagolysosomes under an electron microscope<sup>[38]</sup>. By calculating the LC3-II to LC3-I ratio, the autophagic flux can be quantified<sup>[39]</sup>. In this study, through the detection of changes in LC3-II/LC3-I expression, found that compared with the NC group, the NaIO<sub>3</sub>-induced model indeed exhibited enhanced autophagy. However, upon the addition of the CY-09 and AST, autophagy was reduced, and inflammation was alleviated, and the effect of the drug combination was more

obvious. Autophagosome formation was morphologically examined in 661W cells by transmission electron microscopy, indicating that the NaIO<sub>3</sub>-induced AMD model exhibits enhanced autophagy in photoreceptor cells and that autophagy may play an important role in photoreceptor cell death. In addition, the morphology of autophagosomes was significantly reduced, and autophagic vesicle numbers were decreased when the cells were treated with NLRP3 inhibitors and antioxidants. The retinal thickness of NaIO<sub>3</sub> group was reduced, the a-wave and b-wave of FERG were reduced and visual function was affected. CY-09 alleviated the degree of retinal damage caused by NaIO<sub>3</sub>, and with increasing dose. Reducing the level of NLRP3 can alleviate retinal immune inflammation, and reduce the damage effect. CY-09 alleviates inflammation by inhibiting NLRP3 inflammasome activation<sup>[40-41]</sup>. Activation and assembly of the NLRP3 inflammasome significantly affect the release of IL-1 $\beta$ <sup>[42]</sup>. Antioxidant drugs AST may have the potential to control dry AMD<sup>[43]</sup>. AST has powerful antioxidant, anti-inflammatory, antiapoptotic and immunomodulatory properties<sup>[44]</sup>. AST significantly inhibits the increase in TNF- $\alpha$  and IL-1 $\beta$ , thereby improving inflammation-related diseases<sup>[45]</sup>. After photoreceptor cells are stimulated, NLRP3, caspase-1, IL-1 $\beta$  and IL-18 are activated in the cells. CY-09 and AST inhibits the formation of NLRP3 and promotes autophagy, which can protect photoreceptor cells. These indicate that the NLRP3 and autophagy interact, and one factor can inhibit the other factor to a certain extent, but the overactivation of autophagy can also cause cell death.

In conclusion, *in vitro* treatment with NaIO<sub>3</sub> promoted the expression of NLRP3 in 661W and ARPE-19 cells. The NLRP3 inflammasome may promote the inflammatory death of photoreceptor cells and CY-09 can inhibit NaIO<sub>3</sub>-induced photoreceptor cell damage in the AMD model. By inhibiting the NLRP3 with CY-09 and adding AST, the inflammatory response of photoreceptor cells and RPE cells could be inhibited, resulting in a protective effect. Autophagy and the NLRP3 interact. Autophagy can protect photoreceptor cells, and overactivation of autophagy can cause photoreceptor cell death. Inhibition of the NLRP3 can also inhibit autophagy to a certain extent.

#### ACKNOWLEDGEMENTS

**Authors' contributions:** Wang XL, Gao YX, Yuan QZ, Zhang M contributed to study conception and design and definition of intellectual content. Wang XL was responsible for data analysis and manuscript preparation. Gao YX and Zhang M revised the article critically for important intellectual content. Zhang M is guarantor of this work, who had full access to all the data in this study and take responsibility for the integrity and accuracy of the data. All authors approved the final version of the manuscript.

**Foundations:** Supported by the National Key R&D Project (No.2018YFC1106103); Project of Sichuan Medical Association (No.S22058).

**Conflicts of Interest:** Wang XL, None; Gao YX, None; Yuan QZ, None; Zhang M, None.

#### REFERENCES

- Li JQ, Welchowski T, Schmid M, Mauschitz MM, Holz FG, Finger RP. Prevalence and incidence of age-related macular degeneration in Europe: a systematic review and meta-analysis. *Br J Ophthalmol* 2020;104(8):1077-1084.
- Tan W, Zou J, Yoshida S, Jiang B, Zhou Y. The role of inflammation in age-related macular degeneration. *Int J Biol Sci* 2020;16(15):2989-3001.
- Tolone A, Sen M, Chen Y, Ueffing M, Arango-Gonzalez B, Paquet-Durand F. Pathomechanisms of inherited retinal degeneration and perspectives for neuroprotection. *Cold Spring Harb Perspect Med* 2023;13(6):a041310.
- Thomas CJ, Mirza RG, Gill MK. Age-related macular degeneration. *Med Clin North Am* 2021;105(3):473-491.
- Wong WL, Su X, Li X, Cheung CM, Klein R, Cheng CY, Wong TY. Global prevalence of age-related macular degeneration and disease burden projection for 2020 and 2040: a systematic review and meta-analysis. *Lancet Glob Health* 2014;2(2):e106-e116.
- Liberski S, Wichrowska M, Kocięcki J. Aflibercept versus faricimab in the treatment of neovascular age-related macular degeneration and diabetic macular edema: a review. *Int J Mol Sci* 2022;23(16):9424.
- Chen M, Luo C, Zhao J, Devarajan G, Xu H. Immune regulation in the aging retina. *Prog Retin Eye Res* 2019;69:159-172.
- Medzhitov R. Origin and physiological roles of inflammation. *Nature* 2008;454(7203):428-435.
- Murakami Y, Notomi S, Hisatomi T, Nakazawa T, Ishibashi T, Miller JW, Vavvas DG. Photoreceptor cell death and rescue in retinal detachment and degenerations. *Prog Retin Eye Res* 2013;37:114-140.
- Olivares-González L, Velasco S, Campillo I, Rodrigo R. Retinal inflammation, cell death and inherited retinal dystrophies. *Int J Mol Sci* 2021;22(4):2096.
- Kelley N, Jeltama D, Duan YH, He Y. The NLRP3 inflammasome: an overview of mechanisms of activation and regulation. *Int J Mol Sci* 2019;20(13):3328.
- Li Z, Guo J, Bi L. Role of the NLRP3 inflammasome in autoimmune diseases. *Biomed Pharmacother* 2020;130:110542.
- Zhong C, Wang R, Hua M, Zhang C, Han F, Xu M, Yang X, Li G, Hu X, Sun T, Ji C, Ma D. NLRP3 inflammasome promotes the progression of acute myeloid leukemia via IL-1 $\beta$  pathway. *Front Immunol* 2021;12:661939.
- Hochheiser IV, Behrmann H, Hagelueken G, Rodríguez-Alcázar JF, Kopp A, Latz E, Behrmann E, Geyer M. Directionality of PYD filament growth determined by the transition of NLRP3 nucleation seeds to ASC elongation. *Sci Adv* 2022;8(19):eabn7583.
- Trachalaki A, Tsitoura E, Mastrodimou S, Ivernizzi R, Vasarmidi E, Bibaki E, Tzanakis N, Molyneaux PL, Maher TM, Antoniou K. Enhanced IL-1 $\beta$  release following NLRP3 and AIM2 inflammasome stimulation is linked to mtROS in airway macrophages in pulmonary fibrosis. *Front Immunol* 2021;12:661811.
- Zhang J, Liu X, Wan C, Liu Y, Wang Y, Meng C, Zhang Y, Jiang C. NLRP3 inflammasome mediates M1 macrophage polarization and IL-1 $\beta$  production in inflammatory root resorption. *J Clin Periodontol* 2020;47(4):451-460.
- Muñoz-Planillo R, Kuffa P, Martínez-Colón G, Smith B, Rajendiran T, Núñez G. K<sup>+</sup> efflux is the common trigger of NLRP3 inflammasome activation by bacterial toxins and particulate matter. *Immunity* 2013;38(6):1142-1153.
- Zeng B, Huang Y, Chen S, Xu R, Xu L, Qiu J, Shi F, Liu S, Zha Q, Ouyang D, He X. Dextran sodium sulfate potentiates NLRP3 inflammasome activation by modulating the KCa3.1 potassium channel in a mouse model of colitis. *Cell Mol Immunol* 2022;19(8):925-943.
- Bai D, Du J, Bu X, Cao W, Sun T, Zhao J, Zhao Y, Lu N. ALDOA maintains NLRP3 inflammasome activation by controlling AMPK activation. *Autophagy* 2022;18(7):1673-1693.
- Dominic A, Le NT, Takahashi M. Loop between NLRP3 inflammasome and reactive oxygen species. *Antioxid Redox Signal* 2022;36(10-12):784-796.
- Gupta U, Ghosh S, Wallace CT, Shang P, Xin Y, Nair AP, Yazdankhah M, Strizhakova A, Ross MA, Liu HT, Hose S, Stepicheva NA, Chowdhury O, Nemani M, Maddipatla V, Grebe R, Das M, Lathrop KL, Sahel JA, Zigler JS Jr, Qian J, Ghosh A, Sergeev Y, Handa JT, St Croix CM, Sinha D. Increased LCN2 (lipocalin 2) in the RPE decreases autophagy and activates inflammasome-ferroptosis processes in a mouse model of dry AMD. *Autophagy* 2023;19(1):92-111.
- Lee JJ, Chang-Chien GP, Lin S, Hsiao YT, Ke MC, Chen A, Lin TK. 5-lipoxygenase inhibition protects retinal pigment epithelium from sodium iodate-induced ferroptosis and prevents retinal degeneration. *Oxid Med Cell Longev* 2022;2022:1792894.
- Trojan P, Krauss N, Choe HW, Giessl A, Pulvermüller A, Wolfrum U. Centrin in retinal photoreceptor cells: regulators in the connecting cilium. *Prog Retin Eye Res* 2008;27(3):237-259.
- Borrelli E, Sacconi R, Zuccaro B, Cavalleri M, Bordato A, Zucchiatti I, Querques L, Bandello F, Querques G. Photoreceptor alteration in intermediate age-related macular degeneration. *Sci Rep* 2020;10(1):21036.
- Kaappinen A, Paterno JJ, Blasiak J, Salminen A, Kaarniranta K. Inflammation and its role in age-related macular degeneration. *Cell Mol Life Sci* 2016;73(9):1765-1786.
- Xie SS, Deng Y, Guo SL, Li JQ, Zhou YC, Liao J, Wu DD, Lan WF. Endothelial cell ferroptosis mediates monocrotaline-induced pulmonary hypertension in rats by modulating NLRP3 inflammasome activation. *Sci Rep* 2022;12(1):3056.
- Han X, Sun S, Sun Y, Song Q, Zhu J, Song N, Chen M, Sun T, Xia M, Ding J, Lu M, Yao H, Hu G. Small molecule-driven NLRP3 inflammation inhibition via interplay between ubiquitination and autophagy: implications for Parkinson disease. *Autophagy* 2019;15(11):1860-1881.

- 28 Schnichels S, Paquet-Durand F, Löscher M, Tsai T, Hurst J, Joachim SC, Klettner A. Retina in a dish: Cell cultures, retinal explants and animal models for common diseases of the retina. *Prog Retin Eye Res* 2021;81:100880.
- 29 Lee D, Nakai A, Miwa Y, Negishi K, Tomita Y, Kurihara T. Pemafibrate prevents choroidal neovascularization in a mouse model of neovascular age-related macular degeneration. *PeerJ* 2023;11:e14611.
- 30 Soundara Pandi S, Ratnayaka J, Lotery A, Teeling J. Progress in developing rodent models of age-related macular degeneration (AMD). *Exp Eye Res* 2021;203:108404.
- 31 Enzbrenner A, Zulliger R, Biber J, Pousa AMQ, Schäfer N, Stucki C, Giroud N, Berrera M, Kortvely E, Schmucki R, Badi L, Grosche A, Pauly D, Enzmann V. Sodium iodate-induced degeneration results in local complement changes and inflammatory processes in murine retina. *Int J Mol Sci* 2021;22(17):9218.
- 32 Ren C, Hu C, Wu Y, Li T, Zou A, Yu D, Shen T, Cai W, Yu J. Nicotinamide mononucleotide ameliorates cellular senescence and inflammation caused by sodium iodate in RPE. *Oxid Med Cell Longev* 2022;2022:5961123.
- 33 Zhao J, Kim HJ, Sparrow JR. Multimodal fundus imaging of sodium iodate-treated mice informs RPE susceptibility and origins of increased fundus autofluorescence. *Invest Ophthalmol Vis Sci* 2017;58(4):2152-2159.
- 34 Sekar P, Hsiao G, Chen YS, Lin WW, Chan CM. P2X7 is involved in the mouse retinal degeneration via the coordinated actions in different retinal cell types. *Antioxidants(Basel)* 2023;12(1):141.
- 35 Schnabolk G, Obert E, Banda NK, Rohrer B. Systemic inflammation by collagen-induced arthritis affects the progression of age-related macular degeneration differently in two mouse models of the disease. *Invest Ophthalmol Vis Sci* 2020;61(14):11.
- 36 Chen S, Liu G, Liu X, Wang Y, He F, Nie D, Liu X, Liu X. RNA-seq analysis reveals differentially expressed inflammatory chemokines in a rat retinal degeneration model induced by sodium iodate. *J Int Med Res* 2022;50(8):3000605221119376.
- 37 Balmer J, Zulliger R, Roberti S, Enzmann V. Retinal cell death caused by sodium iodate involves multiple caspase-dependent and caspase-independent cell-death pathways. *Int J Mol Sci* 2015;16(7):15086-15103.
- 38 Hanus J, Anderson C, Sarraf D, Ma J, Wang S. Retinal pigment epithelial cell necroptosis in response to sodium iodate. *Cell Death Discov* 2016;2:16054.
- 39 Ravikumar B, Berger Z, Vacher C, O’Kane CJ, Rubinsztein DC. Rapamycin pre-treatment protects against apoptosis. *Hum Mol Genet* 2006;15(7):1209-1216.
- 40 Blasiak J, Pawlowska E, Chojnacki J, Szczepanska J, Chojnacki C, Kaarniranta K. Zinc and autophagy in age-related macular degeneration. *Int J Mol Sci* 2020;21(14):4994.
- 41 Kaarniranta K, Uusitalo H, Blasiak J, Felszeghy S, Kannan R, Kauppinen A, Salminen A, Sinha D, Ferrington D. Mechanisms of mitochondrial dysfunction and their impact on age-related macular degeneration. *Prog Retin Eye Res* 2020;79:100858.
- 42 Fan Y, Xue G, Chen Q, Lu Y, Dong R, Yuan H. CY-09 inhibits NLRP3 inflammasome activation to relieve pain via TRPA1. *Comput Math Methods Med* 2021;2021:9806690.
- 43 Wang Y, Liu YJ, Zhang MM, Zhou H, Gao YH, Cheng WJ, Ye ZW, Yuan ZY, Xu GH, Li CF, Yi LT. CY-09 alleviates the depression-like behaviors via inhibiting NLRP3 inflammasome-mediated neuroinflammation in lipopolysaccharide-induced mice. *ACS Chem Neurosci* 2022;13(23):3291-3302.
- 44 Chen X, Zhang D, Li Y, Wang W, Bei W, Guo J. NLRP3 inflammasome and IL-1 $\beta$  pathway in type 2 diabetes and atherosclerosis: Friend or foe? *Pharmacol Res* 2021;173:105885.
- 45 Kishimoto Y, Yoshida H, Kondo K. Potential anti-atherosclerotic properties of astaxanthin. *Mar Drugs* 2016;14(2):35.